applied sciences

MDPI

Article

Grain Size Effect in Elution Test of Electric Arc Furnace Slag

Alessandro Riboldi [1], Giovanna Cornacchia [2], Marcello Gelfi [2], Laura Borgese [1], Annalisa Zacco [1], Elza Bontempi [1], Marco V. Boniardi [3], Andrea Casaroli [3] and Laura E. Depero [1,*]

[1] Chemistry for Technologies Laboratory, INSTM and Department of Mechanical and Industrial Engineering, University of Brescia, Via Branze 38, 25123 Brescia, Italy; a.riboldi003@studenti.unibs.it (A.R.); laura.borgese@unibs.it (L.B.); annalisa.zacco@unibs.it (A.Z.); elza.bontempi@unibs.it (E.B.)

[2] Department of Mechanical and Industrial Engineering, University of Brescia, University of Brescia, Via Branze 38, 25123 Brescia, Italy; giovanna.cornacchia@unibs.it (G.C.); marcello.gelfi@unibs.it (M.G.)

[3] Department of Mechanical Engineering, Polytechnic University of Milan, Via La Masa 1, 20156 Milan, Italy; marco.boniardi@polimi.it (M.V.B.); andrea.casaroli@polimi.it (A.C.)

* Correspondence: laura.depero@unibs.it

Received: 12 December 2019; Accepted: 6 January 2020; Published: 9 January 2020

Abstract: In this paper we discuss the effects of deslagging practices and the size of electric arc furnace (EAF) slags on structural, microstructural, composition and leaching tests. The samples were collected from seven steelmakers located in Brescia (Lombardy Region, Italy). Nine granularity fractions of four samples were tested to evaluate the influence of the granularity on the leaching tests. The results showed that, in general, the release of the elements arises when the size of the particle decreases, except in one sample, in which vanadium and zinc displayed the opposite trend. X-ray diffraction results suggest that behavior may be ascribed to the effect of the grinding, which causes a different percentage of the phases in the various fractions. In conclusion, the possible effects of the size should also be carefully considered when defining new leaching test requirements for EAF slags.

Keywords: EAF slag; elemental composition; crystalline phases; leaching test; X-ray diffraction; SEM

1. Introduction

Steel production is one of the most relevant industrial activities in the world. Depending on technologies and processes, about 10–15 wt% of non-metallic solid residue slags are produced [1]. Steel slags are classified as basic oxygen furnace slags, electric arc furnace (EAF) slags and ladle furnace slags [2].

The integrated steelmaking route—producing steel based on the liquid iron originating from iron ore—still dominates the world production of steel, but the EAF route accounts for a larger and larger portion every year. Indeed, it is expected to grow in the next year, to reach 50% of the total steel production.

In the past, steelmakers viewed EAF as inadequate for producing high-quality steel, since the process employs recycled materials. However, EAF has become an efficient and reliable steelmaking alternative. Indeed, today EAF steel cannot be distinguished from steel produced using the integrated blast furnace/oxygen steelmaking route.

Even with continued improvements to the design of steelmaking processes, the steelmaking research community has focused their attention on supply materials and impurity concentration used in steelmaking in order to improve the quality of steel [3–7]. Slag is mainly formed by the lime and the oxygen injected into the steel bath. When the refining process is completed, the slag is removed [8,9]. Due to the physical and mechanical characteristics, slags are widely used in roads and civil constructions,

as concrete aggregates and bituminous mixtures (see for example [8,10–12]). Indeed, it was shown that aggregates containing EAF slags have excellent physical and chemical characteristics, and thus can be used in cement-treated materials [13]. EAF slags are also used in wastewater treatment [14–16], CO_2 sequestration [17], agriculture fertilizer or remedy for soil acidity [18], and reinforcing filler for composite materials [19,20]. The recycling of steel slag may be restricted because of the presence of potentially toxic elements—like Cr, V, Ba and Mo [21]—and leaching tests are mandatory to verify the release of toxic elements in the water [22]. In particular, toxic metal ions can accumulate in the human body and in the environment. A number of studies have been reported to detect and absorb these metals ions [23–25], and different standards and regulations have been adopted to check the possible leaching of the materials. EN 12457:2004 is the adopted standard in Europe and is constituted by four parts, in which different grain sizes and the Liquid/Solid (L/S) ratio are considered. Indeed, the grinding procedure leads to the formation of a variable amount of dust and small particle size that can significantly affect the results [26]. Moreover, the slag chemical composition and phases are also relevant.

Literature reports the effects of slagging procedures on the chemical, mineralogical, morphological structure and leaching [22,27]. The optimization and control of slag composition during the steelmaking process is very difficult because of different factors, as reviewed by Luz et al. [9]. The leaching behavior of aged steel slags has also been reported by Engström et al. [28]. Gelfi et al. [29] showed the effect of rapid cooling on the microstructure of slags and the formation of amorphous slag, determining a low release of Cr in the leaching tests. The release of Ba, V, and Cr have also been related to the presence of a large amount of hydraulic phases, and the addition of SiO_2 during the slagging operation has been suggested [21,30] to promote the formation of gehlenite. Cirilli at al. [31] investigated the leachability of Vanadium, and showed that its leachability is higher in the non-stoichiometric phases. Thus, the formation of stoichiometric tricalcium silicate structures will reduce the leachability of Vanadium.

This paper aims to present and discuss structural, microstructural, composition, and leaching tests of electric arc furnace (EAF) slags obtained by seven steel makers located in Brescia (Italy). Moreover, the influence of the granularity on the leaching tests will also be discussed.

2. Materials and Methods

2.1. Slag Samples

Seven different steel makers located in Brescia provided the carbon steel slags samples. The main differences among their slagging practices are the cooling rate [27] and the addition/no addition of SiO_2 for slag stabilization [30]. The slag samples were divided into three categories depending on the treatment: slagging into a hole and cooling by water jet (slow cooling); slagging on the chute and cooling by water jet (fast cooling); slagging on chute after addiction of SiO_2 and cooling by water jet (fast cooling and modified slag). The samples are classified in Table 1.

Table 1. Description of samples, details of some steel making process parameters (2nd and 3rd column) and slagging procedure (4th column) and grinding size (5th column).

Sample		Steel Type	Furnace Temperature [°C]	Slagging Procedure	Grinding Size	
					4 mm	10 mm
A		Carbon steel 0.167% < C < 0.185%	1550–1620	Fast cooling	X	
B		Carbon steel 0.04% < C < 0.08%	1670–1680	Fast cooling	X	X
C		Carbon steel	1600	Fast cooling	X	X
D	D1	Carbon steel 0.12% < C < 0.18%	1600	Fast cooling and modified slag	X	X
	D2				X	
E	E1	Carbon steel C < 0.25%	1600	Fast cooling and modified slag	X	X
	E2				X	
F		Carbon steel: 0.05% < C < 0.8%	1650	Fast cooling	X	
G		Carbon steel 0.17 < C < 0.19%	1550	Slow cooling	X	

2.2. Chemical and Structural Analysis

The microstructural characterization of slag samples, prepared by the standard metallographic polishing procedure, was performed using LEO EVO 40 XVP scanning electron microscopy (SEM). The elemental semi quantitative analysis was performed using the energy dispersive X-ray spectroscopy (EDXS) microprobe (Link Pentafet Oxford mod 7060). X-ray powder diffraction (XRD) was performed using a Panalytical X' Pert Pro diffractometer, equipped with the X' Celerator detector and Cu anode (Cu Kα = 1.5406 A), operating at 40 KV and 40 mA, allowing the identification of the crystalline phases. The patterns were collected in Bragg Brentano geometry between 5° and 80° (in 2θ). Qualitative analysis of the crystalline phases was achieved by X Pert high score plus database.

2.3. Leaching Tests

Leaching tests of all the samples were performed according to EN12457 2—with a grinding size of 4 mm—and leachate were analyzed by Inductively Coupled Plasma atomic emission spectroscopy (ICP AES). The pH was measured using a Metrohm 827 pH lab pHmeter equipped by a potentiometric electrode. Samples B, C, D, and E were ground at 10 mm (Table 1) to perform the leaching test following EN12457 4. To verify the influence of the size on the leaching, samples B, C, D, and E, after being grounded below 4mm by jaw crusher, were sieved in nine granularity fractions (see Supplementary Material Table S1). Each fraction underwent the leaching test for 24 h and L/S 10 l/Kg, and the leachate were analyzed by Total Reflection X-ray Fluorescence (TXRF) for elemental chemical analysis. TXRF measurements were performed with a Bruker S2 Picofox equipped with Mo tube operating at 50 kV and 750 μA, and a silicon drift detector. Since Gallium was not present in the leachates, 1 mg/L was added as the internal standard for quantification. A volume of 10 μl was deposed on the quartz sample carrier and dried at 50 °C on the heating plate. Three independent specimens were prepared for each sample and measured for 600 s [32].

3. Results

3.1. Morphological, Chemical and Structural Analysis

The EAF slags have a black/grey color, with white spots due to a presence of the calcium carbonate phase. Given its density (between 3.3/3.6 g/cm^3), the high roughness, and porosity, FeO, CaO, SiO_2, Al_2O_3, MgO in a wide range of percentage, 10%–40%, 22%–60%, 6%–34%, 3%–14% and 13%–14%, respectively [8,33], and other minor phases. Ca and Si mainly originate from the inert materials added to the steel bath, while the presence of other elements, such as Cr, Ti, and Cu, is due to impurities of the ferrous scraps. Larnite ($2CaO\text{-}SiO_2$), brownmillerite ($Ca_2(Al,Fe)_2O_5$), wustite (FeO), calcium silicate, silicon aluminates, gehlenite ($Ca_2Al[AlSiO_7]$), bredigite ($Ca_7Mg(SiO_4)_4$), magnetite (Fe_3O_4), magnesioferrite ($MgFe_2O_4$) and manganese oxides are the crystalline phases usually identified by XRD. The composition and the phases of the slags are related to the cooling rate, the metal scrap, and the feature of steel plant [34]. A high variability was also observed in slags collected from the steel plant at different times.

The slag samples were classified according to the slagging operation, showing that, when SiO_2 is added, the slag appears less porous and dusty, as shown (see Figure 1).

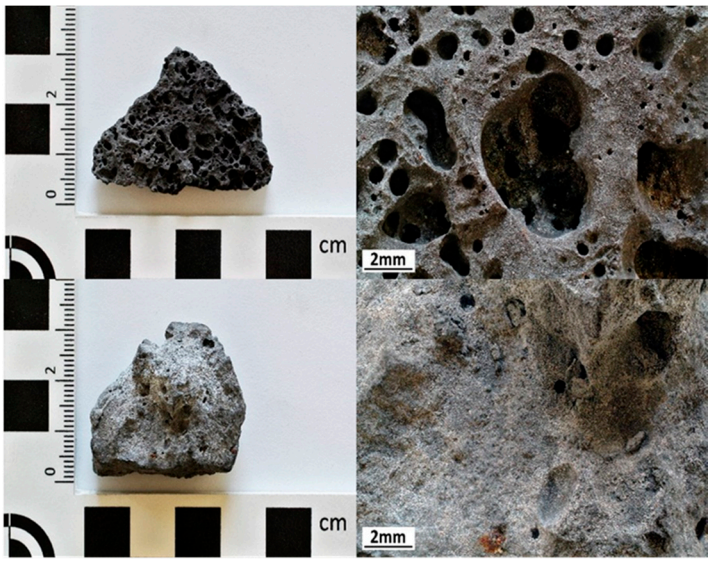

Figure 1. Photo of low cooling rate slag (top, sample G) and SiO_2 modified slag (bottom, sample D1). Reproduced in colors.

Morphological and compositional analyses have been performed to evaluate the differences among the samples. In the SEM micrographs collected in back scattering modes (see Figure 2), the differences in the morphology and contrast can be related to the phases. Grains are formed during the solidification of the liquid slag and correspond to different phases [35].

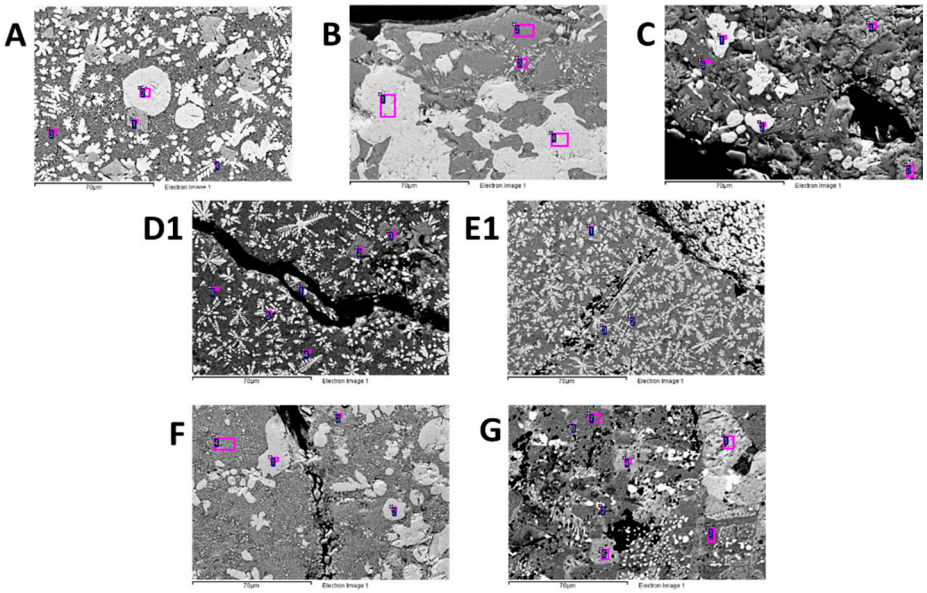

Figure 2. SEM micrographs of samples **A**, **B**, **C**, **D1**, **E1**, **F** and **G**. Numbered purple squares represent the position where Energy Dispersive X-ray Spectroscopy (EDXS) measurements are collected. Reproduced in black and white.

Indeed, non-uniform solidification occurs in the solid slag because of the temperature gradient in the matrix: high melting point phases—such as silicates—solidify first, giving rise to grain structures with shapes typical of the phase composition [30]. EDXS measurements (Table 2) allowed us to identify the phases in the slags, that were confirmed by XRD analysis (see Supplementary Material Figure S1). Analogies and differences among samples can be associated with the parameters of the solidification process, in particular the cooling rate and the SiO_2 addition. In all the samples, a high percentage of

a dark matrix is present, with a high content of Si, Ca and also few percentages of Fe and Al. The content of the last two elements is related to the larnite and gehlenite phases percentages, as detected by XRD. In particular, the larnite content is significant in the samples that undergo slow cooling, while the amount of gehlenite is high in the case of fast cooling and SiO_2 addition. The light matrix has a dendritic structure, with rounded and sharp edged grains. Dendritic and rounded grains have a high content of Fe with the presence of Mg and Cr. The composition of the rounded grains is compatible with iron oxides as magnesioferrite, while the phase of the dendritic structures is attributed to the wustite phase. Dendritic structures are present in the samples obtained in the fast cooling process (A, C, F, D1 and E1), and they are in a more significant percentage in the sample obtained by adding silica (D, E). In the latter case, the dendritic structure formation may be related to a reduction in the slag melting temperature induced by the SiO_2 [30]. The slower is the cooling rate, the larger is the size of round shape grains (see samples A, B and G). Grains with sharp edges have a high content of Cr, and they are found only in the fast cooled samples, in which the crystalline magnesiochromite phase is also present.

Table 2. Results of EDXS analysis expressed as mole percentage ratio per sample measurement position and the corresponding crystalline phase identification.

Sample	Position	O	Mg	Al	Si	Ca	Ti	Cr	Mn	Fe	Phases Identification
		Concentration [Mol/Mol%]									
A	1	43.9	12.3	11.7	-	0.4	-	21.6	2.2	7.8	Magnesiochromite
	2	38.6	21.3	0.7	-	0.4	-	4.0	4.1	30.8	Magnesioferrite
	3	47.4	0.7	14.4	11.0	25.2	0.5	-	0.6	5.8	Gehlenite
	4	39.8	9.5	3.0	1.1	3.3	-	0.8	5.0	36.7	Wuestite
B	1	42.3	12.2	1.5	0.0	1.2	0.0	2.0	6.5	34.3	Magnesioferrite
	2	53.5	-	-	16.6	29.4	-	-	-	0.4	Larnite
	3	48.0	0.9	19.7	3.1	19.0	0.8	-	0.8	7.7	Gehlenite
	4	40.1	14.3	1.6	-	1.1	-	2.9	6.1	33.9	Magnesioferrite
C	1	40.3	-	-	-	0.3	-	0.4	11.9	34.7	Wuestite
	2	41.2	-	-	-	0.5	-	-	12.4	32.9	Wuestite
	3	49.3	11.3	11.3	-	0.7	-	20.2	3.2	4.7	Magnesiochromite
	4	51.0	13.0	13.0	-	0.4	-	17.8	3.0	4.3	Magnesiochromite
	5	50.7	4.6	4.6	14.7	23.4	0.5	-	1.1	2.8	Gehlenite
D1	1	54.6	2.0	6.9	11.6	19.2	0.3	-	0.9	4.5	Gehlenite
	2	48.5	8.8	12.3	-	0.5	-	19.1	2.5	8.3	Magnesiochromite
	3	47.3	9.2	13.0	-	0.7	-	18.9	2.5	8.5	Magnesiochromite
	4	50.6	1.8	9.0	11.9	20.0	0.5	-	0.8	5.5	Gehlenite
	5	44.2	7.1	2.1	2.3	4.5	-	-	5.7	34.3	Wuestite
	6	49.2	1.6	12.8	10.6	17.6	-	-	1.2	6.9	Gehlenite
E1	1	49.4	9.2	16.6	-	1.0	-	13.5	2.3	7.9	Magnesiochromite
	2	51.4	2.4	9.0	14.5	17.7	-	-	0.7	4.2	Gehlenite
	3	47.2	5.2	5.2	7.0	8.6	0.4	0.6	3.8	22.0	Wuestite
F	1	45.9	20.1	3.3	-	-	-	-	3.7	24.7	Wuestite
	2	47.0	20.8	2.0	-	-	-	1.6	3.5	25.0	Wuestite
	3	53.0	13.0	11.3	-	0.5	-	15.9	1.3	5.0	Magnesiochromite
	4	55.4	2.0	8.7	11.5	15.9	-	-	0.5	6.1	Gehlenite
G	1	51.1	4.2	0.0	16.6	17.4	0.0	-	3.6	7.2	Larnite
	2	43.2	6.7	0.0	0.0	0.9	0.0	-	7.3	41.9	Wuestite
	3	53.8	2.2	11.0	13.9	17.3	0.0	-	0.4	1.4	Gehlenite
	4	53.9	4.7	0.0	16.2	16.0	0.4	-	2.7	6.1	Larnite
	5	53.5	4.1	0.0	16.0	16.1	0.3	-	3.3	6.7	Larnite
	6	50.3	4.5	0.7	16.7	16.9	0.5	-	3.4	7.0	Larnite
	7	52.5	2.6	10.2	14.9	18.1	0.0	-	0.4	1.3	Gehlenite

3.2. Leaching Test

National legislations regulate the procedures for the leaching test as well as the physical and chemical analysis of the slags. The results are usually compared with the limit values and depend upon the final destination of the materials. The pH value of the leachates is between 9 and 11, and the correlation with the process parameters is not significant. The results of the Inductively Coupled Plasma Optical Emission Spectroscopy (ICP-AES) analysis are reported in Table 3. The relative standard deviation (RSD) of the data is fixed at 10%. For the identified elements, four concentration ranges can

be identified: above 1 mg/L are detected for Ca, Si, K and Ba; between 0.1 and 1 mg/L for Sr, V and Mo; between 10 µg/L and 100 µg/L for P, Cr, Fe, Co, Zn, Se and Rb; less than 10 µg/L for Mn, Cu, In, Pb and Cd. The higher is the pH the higher is the release of Ba.

Table 3. ICP-AES measurements results on leachate according to EN12457 2.

	A	B	C	D1	E1	F	G
Elements	**Conc. [mg/L]**						
Si	1.3	1.0	0.2	8.0	11.8	7.8	0.7
P	0.01	0.005	0.005	0.01	0.008	0.008	0.006
K	0.3	0.08	0.2	0.7	5.3	1.0	3.0
Ca	58.2	84.6	152.2	27.6	21.9	29.7	66.5
V	0.1	0.03	0.01	0.1	0.06	0.2	0.03
Cr	0.002	0.02	0.004	0.001	-	0.006	0.001
Mn	0.001	0.001	0.001	0.001	0.001	0.001	0.002
Fe	0.02	0.02	0.03	0.004	0.005	0.004	0.02
Co	0.005	0.005	0.02	-	0.004	-	0.01
Cu	-	-	-	-	-	0.001	-
Zn	0.01	0.01	0.01	0.006	0.007	0.002	0.01
Se	0.007	0.009	0.01	0.004	0.01	0.007	0.01
Rb	0.01	0.02	0.01	0.02	0.03	0.01	0.02
Sr	0.1	0.1	0.5	0.1	0.2	0.1	0.1
Mo	0.07	0.06	0.07	0.05	0.2	0.06	0.2
Cd	-	-	-	-	-	-	-
In	0.003	0.001	0.002	0.003	-	0.002	0.002
Ba	0.6	0.2	2.0	0.5	0.8	0.2	1.1
Pb	0.005	0.004	-	0.005	0.003	0.004	-

The intrinsic variability of leaching tests of the same sample (intra-sample variability) has been evaluated for SiO_2 stabilized slag (namely D and E). Samples D1-D2 and E1-E2 were collected from two different plants in two different days. The leaching test results have been compared in terms of average values and relative standard deviations (RSD%) (Table 4). A high variability in the results is observed, probably due to the sampling or to the furnace feeding. In general, the RSD is high when the element concentration is low. Indeed, descriptive statistics, in terms of minimum and maximum RSD range, per each concentration class defined above, highlights an inverse relationship with the concentration. A higher variability is observed in samples E1 E2 than in samples D1 D2. The intra-sample variability is similar to that observed among the samples (see Supplementary Material Table S2). The same result was obtained with samples of different plants. The principal components analysis confirms the absence of any correlation among samples belonging to the same cooling rate category.

The analysis of samples B, C, D1, and E1 have been repeated with the same standard procedure (UNI EN 12,457 2) in a second laboratory to check the repeatability of the test. Results obtained by the two laboratories are not different, suggesting that the primary source of variability is the sample non-homogeneity (see Supplementary Material Table S3).

To evaluate the effect of the grain size on the leaching test results, two granularities—4 and 10 mm, respectively—are considered according to EN 12,457 Part 2 and Part 4. The results of samples B, C, D1 and E1 are reported in Table 5. For most of the elements, the highest concentrations are found in the specimens with the lowest granularity, possibly related to their high surface area.

Table 4. Intra-sample variability expressed as the average and relative standard deviations (RSD%) (in brackets) of elemental concentration measured in leachates from samples D1-D2 (second column) and samples E1-E2 (third column).

	Sample D1-D2	Sample E1-E2
Elements	**Conc. [mg/L] (RSD%)**	
Si	8.8 (12.8)	12.6 (8.9)
P	0.01 (0.5)	0.007 (18)
K	0.6 (21.2)	4.7 (18.3)
Ca	27.3 (1.8)	27.2 (27.3)
V	0.14 (18.2)	0.08 (25.9)
Cr	0.002 (38.6)	0.0005 (141.4)
Mn	0.001 (6.7)	0.001 (23.4)
Fe	0.003 (27.8)	0.003 (84.4)
Co	-	0.003 (39.5)
Zn	0.003 (129.2)	0.007 (7.6)
Se	0.004 (3.7)	0.01 (27.5)
Rb	0.01 (23.8)	0.03 (9.1)
Sr	0.11 (25.4)	0.19 (22.9)
Mo	0.05 (25.4)	0.14 (39.2)
In	0.003 (25.0)	-
Ba	0.5 (2.8)	0.6 (46.6)
Pb	0.002 (141.4)	0.002 (141.4)

Table 5. Elemental concentration in leachates from samples B, C, D1 and E1 with and ICP-AES results on 4 and 10 mm granularity.

	B		C		D1		E1	
	4 mm	**10 mm**	**4 mm**	**10 mm**	**4 mm**	**10 mm**	**4 mm**	**10 mm**
Elements	**Conc. [mg/L]**							
Ba	0.24	0.12	1.08	0.97	0.46	0.44	0.81	0.94
Zn	-	-	-	-	-	-	-	-
Co	-	-	-	-	-	-	-	-
V	0.021	0.088	0.028	0.053	0.116	0.107	0.074	0.049
Cr	0.021	0.018	0.005	0.018	-	-	-	-
Se	0.002	0.001	0.003	0.001	-	-	-	-
Mo	0.0869	0.027	0.0541	0.039	0.04	0.021	0.1642	0.16
Fe	-	-	0.0271	0.024	-	-	-	-
Mn	-	-	-	-	-	-	-	-
RSD 10%								

To confirm the grain sizes effect on the leaching test, samples B, C, D1 and E1 were selected and their 4 mm granularity specimens were sieved and partitioned in nine granularity fractions. Finally, the leaching test procedure was performed on each fraction. Because of the high number of leachates, for the elemental analysis, the fast and cheap Total reflection X-ray fluorescence (TXRF) technique was used. We considered Ca, Zn, Sr, V and Ba, whom concentration can be reliably determined (comparison among ICP-AES and TXRF data is reported in Supplementary Material Table S4). The TXRF results of the nine fractions are reported in Figure 3 (all the data are reported in Supplementary Material Table S5). For each element, the concentrations have been normalized to the maximum obtained in the nine fractions. In samples B and C, the general trend confirms that the leaching of the elements arises when the grain size decreases, except in the case of V and Zn for sample B, that have an opposite trend. In sample D1 and E1, the monotone behavior is not clear. Both these results suggest a different phase composition of the fractions, as supported by XRD analysis (see Supplementary Material Figure S2). We suggest that the different percentage of the crystalline phases in the fractions can be determined

by the differences in their mechanical behavior. Indeed, the grinding procedure affects differently on the hard and fragile phases, leading to a different phase and elemental composition of particles with different sizes. The different solubility of hard and fragile phases will reflect in the leachate composition. This result may also be due to the common ion effect on the solubility of some elements, which may determine their re-precipitation [36].

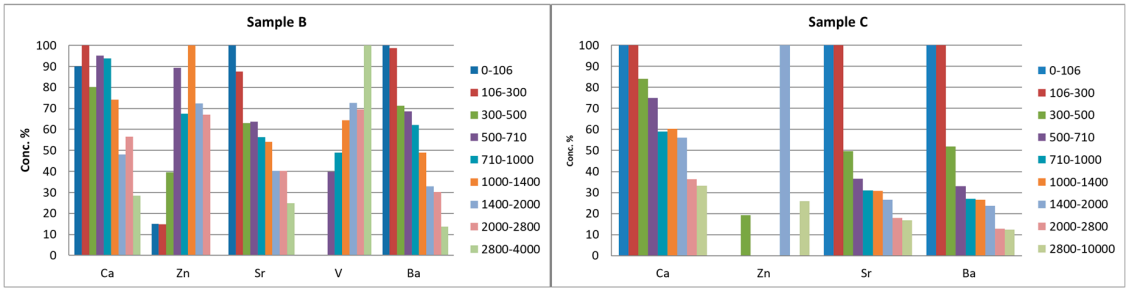

Figure 3. Normalized elements concentration of Ca, Zn, Sr, V and Ba measured by TXRF, in leachates from samples B, C. Reproduced in Colors.

4. Conclusions

The structure, microstructure and leaching behavior of EAF slags from seven different steel makers located in Brescia have been studied and their relationship with the parameters of the slagging procedure are discussed. We showed that, when silica is added during the slagging procedure, slags have low porosity and smooth surfaces. The element concentrations in the leaching tests samples are not significantly related to the slagging parameters and their high variability is mostly due to the furnace feeding and sampling.

The influence of the granularity on leaching has been checked by sieving four samples in nine granularity fractions. In general, the results showed a positive trend with surface area and the element content, with the exception of V and Zn in one sample. This result is likely due to the effect of the grinding on phases, which will cause a higher percentage of hard phases in large grains. Indeed, this difference on phase percentages will change the solubility equilibrium of the leachates. Studies are in progress to demonstrate the correlation between the element concentrations in the leaching tests and the phase composition of the slags.

New leaching test requirements for EAF slags must consider the effects due to the grain size, particularly when grinding is necessary for their uses.

Supplementary Materials: The following are available online at http://www.mdpi.com/2076-3417/10/2/477/s1, Figure S1: XRD patterns of samples A, B, C, D1, E1, F and G, with the corresponding phase identification, Figure S2: XRD patterns collected on Fractions of the lowest (blue) and highest (black) size fraction of sample B, Table S1: Granularity fraction sizes, Table S2: Intra-sample and inter-sample RSD% variability, Table S3: Leaching test results performed in different laboratories, Table S4: Comparison between leaching test results performed by ICP-AES and TXRF, Table S5: Leaching test results performed by TXRF on the different granularity fractions.

Author Contributions: Conceptualization, A.R., L.B. and L.E.D.; methodology, A.R., L.B., L.E.D.; software, A.R., G.C., M.G., and A.Z.; investigation, A.R., A.Z., G.C., M.G., A.C.; writing—original draft preparation, A.R.; writing—review and editing, L.B., A.C., M.V.B., E.B., G.C., M.G.; supervision, L.E.D.; project administration, L.E.D.; funding acquisition, L.E.D. All authors have read and agree to the published version of the manuscript.

Funding: This research was funded by Regione Lombardia Cariplo Foundation 19037, 18-12-2018 on B.U.R.L. n°52, 27-12-2018, grant n° 2018-1733, project "Development of novel slag based glass ceramic for plasma spray coating and 3D printing—3D SLAG", CUP E83D18000240009.

Acknowledgments: The authors acknowledge RAMET consortium (Environmental Research for Metallurgy) for providing the samples and Eng. Alessandro Corsini for useful discussion.

Conflicts of Interest: The authors declare no conflict of interest.

References

1. Proctor, D.M.; Fehling, K.A.; Shay, E.C.; Wittenborn, J.L.; Green, J.J.; Avent, C.; Bigham, R.D.; Connolly, M.; Lee, B.; Shepker, T.O.; et al. Physical and chemical characteristics of blast furnace, basic oxygen furnace, and electric arc furnace steel industry slags. *Environ. Sci. Technol.* **2000**, *34*, 1576–1582. [CrossRef]
2. Yi, H.; Xu, G.; Cheng, H.; Wang, J.; Wan, Y.; Chen, H. An Overview of Utilization of Steel Slag. *Procedia Environ. Sci.* **2012**, *16*, 791–801. [CrossRef]
3. Chen, W.; Yin, X.; Ma, D. A bottom-up analysis of China's iron and steel industrial energy consumption and CO_2 emissions. *Appl. Energy* **2014**, *136*, 1174–1183. [CrossRef]
4. Hickey, K.D. Danieli 2010–2011 technology report. *Iron Steel Technol.* **2012**, *9*, 136–137.
5. Argenta, P.; Guzzon, M. Techint's latest developments in EAF environmental-friendly technologies. *Steel Times Int.* **2006**, *30*, 44.
6. Fruehan, R.J. New steelmaking processes: Drivers, requirements and potential impact. *Ironmak. Steelmak.* **2005**, *32*, 3–8. [CrossRef]
7. Narholz, T.; Villemin, B. The new VAI FUCHS ultimate EAF: Dawn of a new era in electric steelmaking. *Metall. Ital.* **2005**, *97*, 72–74.
8. Yildirim, I.Z.; Prezzi, M. Chemical, Mineralogical, and Morphological Properties of Steel Slag. *Adv. Civ. Eng.* **2011**, *2011*. [CrossRef]
9. Luz, A.P.; Tomba Martinez, A.G.; López, F.; Bonadia, P.; Pandolfelli, V.C. Slag foaming practice in the steelmaking process. *Ceram. Int.* **2018**, *44*, 8727–8741. [CrossRef]
10. Motz, H.; Geiseler, J. Products of steel slags an opportunity to save natural resources. *Waste Manag.* **2001**, *21*, 285–293. [CrossRef]
11. Jiang, Y.; Ling, T.C.; Shi, C.; Pan, S.Y. Characteristics of steel slags and their use in cement and concrete—A review. *Resour. Conserv. Recycl.* **2018**, *136*, 187–197. [CrossRef]
12. Skaf, M.; Manso, J.M.; Aragón, Á.; Fuente-Alonso, J.A.; Ortega-López, V. EAF slag in asphalt mixes: A brief review of its possible re-use. *Resour. Conserv. Recycl.* **2017**, *120*, 176–185. [CrossRef]
13. Autelitano, F.; Giuliani, F. Electric arc furnace slags in cement-treated materials for road construction: Mechanical and durability properties. *Constr. Build. Mater.* **2016**, *113*, 280–289. [CrossRef]
14. Oh, C.; Rhee, S.; Oh, M.; Park, J. Removal characteristics of As(III) and As(V) from acidic aqueous solution by steel making slag. *J. Hazard. Mater.* **2012**, *213*, 147–155. [CrossRef]
15. Kim, D.H.; Shin, M.C.; Choi, H.D.; Seo, C.I.; Baek, K. Removal mechanisms of copper using steel-making slag: Adsorption and precipitation. *Desalination* **2008**, *223*, 283–289. [CrossRef]
16. Beh, C.L.; Chuah, T.G.; Nourouzi, M.N.; Choong, T.S.Y. Removal of heavy metals from steel making waste water by using Electric Arc Furnace slag. *J. Chem.* **2011**, *9*, 2557–2564. [CrossRef]
17. Sun, Y.; Yao, M.S.; Zhang, J.P.; Yang, G. Indirect CO_2 mineral sequestration by steelmaking slag with NH_4Cl as leaching solution. *Chem. Eng. J.* **2011**, *173*, 437–445. [CrossRef]
18. Wang, X.; Cai, Q.-S. Steel Slag as an Iron Fertilizer for Corn Growth and Soil Improvement in a Pot Experiment. *Pedosphere* **2006**, *16*, 519–524. [CrossRef]
19. Cornacchia, G.; Agnelli, S.; Gelfi, M.; Ramorino, G.; Roberti, R. Reuse of EAF Slag as Reinforcing Filler for Polypropylene Matrix Composites. *JOM* **2015**, *67*, 1370–1378. [CrossRef]
20. Ter Teo, P.; Seman, A.A.; Basu, P.; Sharif, N.M. Characterization of EAF Steel Slag Waste: The Potential Green Resource for Ceramic Tile Production. *Procedia Chem.* **2016**, *19*, 842–846. [CrossRef]
21. Mombelli, D.; Mapelli, C.; Di Cecca, C.; Barella, S.; Gruttadauria, A. Electric arc furnace slag: Study on leaching mechanisms and stabilization treatments. *Metall. Ital.* **2016**, *108*, 5–17.
22. Chand, S.; Chand, S.K.; Paul, B.; Kumar, M. Long-term leaching assessment of constituent elements from Linz–Donawitz slag of major steel industries in India. *Int. J. Environ. Sci. Technol.* **2018**, *16*, 6397–6404. [CrossRef]
23. Awual, M.R.; Hasan, M.M.; Eldesoky, G.E.; Khaleque, M.A.; Rahman, M.M.; Naushad, M. Facile mercury detection and removal from aqueous media involving ligand impregnated conjugate nanomaterials. *Chem. Eng. J.* **2016**, *290*, 243–251. [CrossRef]
24. Awual, M.R.; Hasan, M.M.; Khaleque, M.A.; Sheikh, M.C. Treatment of copper(II) containing wastewater by a newly developed ligand based facial conjugate materials. *Chem. Eng. J.* **2016**, *288*, 368–376. [CrossRef]

25. Awual, M.R.; Khraisheh, M.; Alharthi, N.H.; Luqman, M.; Islam, A.; Rezaul Karim, M.; Rahman, M.M.; Khaleque, M.A. Efficient detection and adsorption of cadmium(II) ions using innovative nano-composite materials. *Chem. Eng. J.* **2018**, *343*, 118–127. [CrossRef]
26. Barella, S.; Gruttadauria, A.; Magni, F.; Mapelli, C.; Mombelli, D. Survey about Safe and Reliable Use of EAF Slag. *ISIJ Int.* **2012**, *52*, 2295–2302. [CrossRef]
27. Tossavainen, M.; Engstrom, F.; Yang, Q.; Menad, N.; Lidstrom Larsson, M.; Bjorkman, B. Characteristics of steel slag under different cooling conditions. *Waste Manag.* **2007**, *27*, 1335–1344. [CrossRef]
28. Engström, F.; Larsson, M.L.; Samuelsson, C.; Sandström, Å.; Robinson, R.; Björkman, B. Leaching behavior of aged steel slags. *Steel Res. Int.* **2014**, *85*, 607–615. [CrossRef]
29. Gelfi, M.; Cornacchia, G.; Roberti, R. Investigations on leaching behavior of EAF steel slags. In Proceedings of the Euroslag 2010, Madrid, Spain, 20–22 October 2010; pp. 1–12.
30. Mombelli, D.; Mapelli, C.; Barella, S.; Gruttadauria, A.; Le Saout, G.; Garcia-Diaz, E. The efficiency of quartz addition on electric arc furnace (EAF) carbon steel slag stability. *J. Hazard. Mater.* **2014**, *279*, 586–596. [CrossRef] [PubMed]
31. Cirilli, F.; Di Donato, A.; Di Sante, L.; Martini, U.; Miceli, P. V leaching in EAF slags. In Proceedings of the EUROSLAG 2015, Linz, Austria, 21–23 October 2015.
32. Borgese, L.; Dalipi, R.; Riboldi, A.; Bilo, F.; Zacco, A.; Federici, S.; Bettinelli, M.; Bontempi, E.; Depero, L.E. Comprehensive approach to the validation of the standard method for total reflection X-ray fluorescence analysis of water. *Talanta* **2018**, *181*, 165–171. [CrossRef]
33. Pellegrino, C.; Gaddo, V. Mechanical and durability characteristics of concrete containing EAF slag as aggregate. *Cem. Concr. Compos.* **2009**, *31*, 663–671. [CrossRef]
34. Street, A. Variability of chemical composition of metallurgical slags after steel production. *RMZ Mater. Geoenviron. Mater. Geookolje* **2013**, *60*, 263–270.
35. Liu, L.; Hu, M.L.; Bai, C.G.; Lü, X.W.; Xu, Y.Z.; Deng, Q.Y. Effect of cooling rate on the crystallization behavior of perovskite in high titanium-bearing blast furnace slag. *Int. J. Miner. Metall. Mater.* **2014**, *21*, 1052–1061. [CrossRef]
36. Apul, D.S.; Gardner, K.H.; Eighmy, T.T.; Fällman, A.M.; Comans, R.N.J. Simultaneous application of dissolution/precipitation and surface complexation/surface precipitation modeling to contaminant leaching. *Environ. Sci. Technol.* **2005**, *39*, 5736–5741. [CrossRef] [PubMed]